Superconducting properties of a single-crystal sphere of $ErRh_4B_4$

F. Behroozi*
Biomolecular Engineering Branch, Naval Research Laboratory, Washington, D.C. 20375

L. N. Hall,† G. W. Crabtree, and D. G. Hinks
Materials Science Division, Argonne National Laboratory, Argonne, Illinois 60439
(Received 3 April 1989)

We report on the superconducting and magnetic properties of a single-crystal sphere of the primitive tetragonal phase of $ErRh_4B_4$. Our data consist of magnetization and susceptibility measurements in fields up to 50 kOe and at temperatures down to 0.4 K. The crystal exhibits extreme anisotropy in its response to a magnetic field. It is a weak paramagnet when the external field is along the tetragonal $\bar{c}$ axis but reverts to a strong paramagnet when the field is in the basal plane. The magnetization curves reveal a first-order phase transition at H_{c2} when the field is in the basal plane. Evidence for a temperature domain in which superconductivity and long-range ferromagnetic order appear to coexist is also presented. The magnetization curves are further analyzed to obtain the critical fields, the Ginzburg-Landau parameters, Curie plot, and the ferromagnetic moment of the system.

I. INTRODUCTION

It is well known[1] that three distinct crystalline phases exist for $ErRh_4B_4$: orthorhombic ($T_c=4.5$ K, $T_N=0.3$ K), body-centered tetragonal ($T_c=7.8$ K, $T_N=0.65$ K), and primitive tetragonal ($T_c=8.6$ K, $T_f=0.7$ K). Here T_c refers to the superconducting transition temperature, T_N to the Néel temperature, and T_f denotes the ferromagnetic transition temperature. All three structures share a weak coupling between the magnetic moments (erbium $4f$ electrons) and the conduction electrons (rhodium $4d$ electrons). Consequently, the interaction between the conduction electrons and the erbium moments (denoted by s-f interaction) is very weak becoming important only at temperatures below 1 K. As a result all three phases exhibit superconductivity. However, as the temperature is lowered below 1 K, the magnetic lattice orders antiferromagnetically in the orthorhombic and bct (body-centered-tetragonal) structures with superconductivity persisting. In contrast, the primitive tetragonal structure reenters a normal ferromagnetic phase accompanied by the destruction of superconductivity when the temperature is lowered through T_f. For a small temperature interval $\Delta T\cong 0.3$ K above T_f, there is strong evidence for the coexistence of superconductivity and long-range ferromagnetic order.[2] Whereas the coexistence of superconductivity and antiferromagnetism is rather common, the tetragonal phase of $ErRh_4B_4$ and the Chevrel phase of $HoMo_6S_8$ are so far the only compounds which exhibit the coexistence of superconductivity and ferromagnetic order unequivocally.[3] Due to these intriguing properties the primitive tetragonal phase of $ErRh_4B_4$ has attracted the most attention.

Previous work has shown that in the primitive tetragonal phase, the Er moments are confined to the basal plane by strong crystal-field effects.[4] As a result, the tetragonal axis is the magnetically hard direction, while the two equivalent a axes in the basal plane are the easy magnetic directions along which the Er moments readily align. Consequently, the crystal exhibits great anisotropy in its response to an external magnetic field.[5] To study the magnetic behavior of the reentrant phase of the $ErRh_4B_4$ system in any detail, it is therefore essential to perform the measurements on a single-crystal specimen. Most of the magnetic studies reported in the literature[6] are, however, on polycrystalline specimens, which necessarily describe the polycrystalline average of the magnetic properties and often mask the unusual and highly interesting properties of the system.

In this paper we report on the superconducting and magnetic properties of a single-crystal sphere of the primitive tetragonal phase of $ErRh_4B_4$. Our data consist of ac and dc magnetization and susceptibility measurements in fields up to 50 kOe and in temperatures down to 0.4 K. Following the introduction, the experimental method and typical data are presented in Sec. II. In Sec. III we describe the superconducting properties of the system for $T_c > T > T_f$ and in Sec. IV we briefly review the magnetic behavior of the system in paramagnetic and ferromagnetic phases.

II. EXPERIMENTAL DETAILS

The single crystal was grown by solidification of a nonstoichiometric Er-Rh-B melt. The ingot contained a bicrystal which was cut along its grain boundary to yield two single crystals. The larger was used for neutron-diffraction experiments, while part of the small crystal was used to form a sphere of diameter approximately equal to 1 mm with less than 5% variation in its radius for the work presented here. For a spherical sample, the internal field H_i is related to the applied field H_a by the relation

$$H_i = H_a - 4\pi n M \ ,$$

for all crystallographic directions. In this expression M is the magnetization and n is the demagnetizing factor, which for a sphere equals $\frac{1}{3}$.

To obtain the magnetization curves, the specimen is placed within one of two identical opposing coils. With the magnetic field increasing at a constant rate, the net signal from the two coils is proportional to the magnetic susceptibility of the specimen. Time integration of this net signal yields the magnetization as a function of the applied field.[7]

Figure 1 shows the dc magnetization curve for the specimen at $T=4$ K with the external field parallel to the crystallographic $\bar{a}$ direction. Since the Er moments align readily in this field configuration, the crystal shows a large magnetic response. To generate data for a complete field cycle, we begin with a demagnetized sample at $H_a=0$, $M=0$, and proceed to increase the field uniformly to about 5 kOe, then decrease it to -5 kOe, and increase it again to 5 kOe. Further cycling of the field retraces the outer hysteretic loop. The magnetization curve beginning at $H_a=M=0$ and ending at $H_a=5$ kOe will be referred to as the initial or virgin curve.

In discussing the magnetization curves of our spherical sample ($n=\frac{1}{3}$), it will be helpful to keep in mind the change of appearance in the curves due to the specimen's finite demagnetization factor. In general, for a specimen having a demagnetization factor n, the Meissner slope is given by

$$\frac{dM}{dH_a} = -1/[4\pi(1-n)] \ ,$$

while a discontinuous change in the magnetization (as in a first-order phase transition) is characterized by a line with a constant slope of

$$\frac{dM}{dH_a} = -1/n \ .$$

Moreover, the magnetization curves for $n \neq 0$ case can be always reduced to the case of $n=0$ by noting that

$$H_i = H_a - 4\pi n M \ ,$$

where the internal field H_i is identical to the field experienced by a specimen in the form of a long needle oriented along the external field for which $n=0$.

For an ellipsoidal sample which exhibits a Meissner slope as well as a first-order magnetic phase transition, the two slope requirements uniquely determine both the magnetization scale and the demagnetizing factor. In our case where the demagnetizing factor is well known from the geometry, the above constraints provide a severe test of the consistency of the data.

Figure 2 shows schematically the magnetization curves expected for a long needle-shaped specimen ($n=0$, dashed line) compared to that for a spherical sample ($n=\frac{1}{3}$, solid line), with hypothetical first-order phase transitions at H_{c1} and H_{c2}. A paramagnetic normal state is assumed. As expected, the two field points for which $M=0$, remain unchanged. However, all other points of the solid curve shift relative to the dashed curve.

A noteworthy feature of Fig. 2 is that the superconducting Gibbs free energy density relative to the normal state is given by

$$(G-G_n) = \int_0^{H_{c2}} (M-M_n)dH$$

and may be computed using either of the two curves since the above expression gives the same result for both curves. We also note in passing that the latent heats associated with the first-order phase transitions at H_{c1} and H_{c2} are given by

$$L_1 = T\Delta M_1 (dH_{c1}/dT)$$

and

$$L_2 = T\Delta M_2 (dH_{c2}/dT) \ ,$$

where ΔM_1 and ΔM_2 are the discontinuity in magnetization at H_{c1} and H_{c2}, respectively.

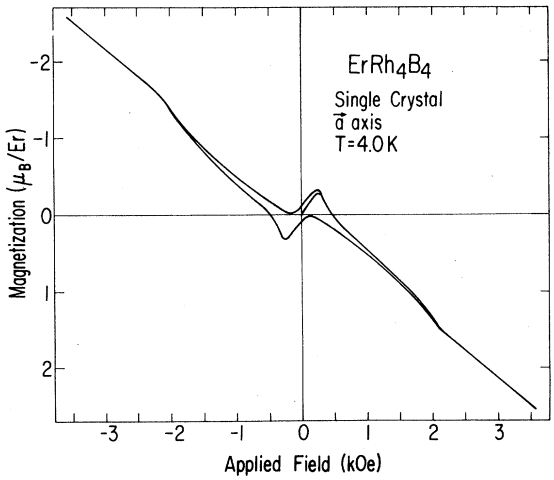

FIG. 1. Magnetization curve at $T=4$ K. The external field is parallel to the crystallographic $\bar{a}$ direction.

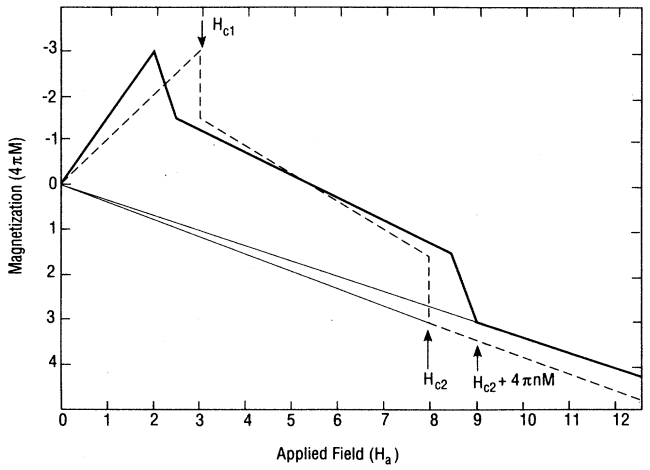

FIG. 2. Schematic magnetization curves for a long needle-shaped specimen (dashed line), and a spherical sample (solid line). Hypothetical first-order phase transitions are assumed at H_{c1} and H_{c2} to illustrate their signatures. The normal state is assumed to be paramagnetic.

III. SUPERCONDUCTING PROPERTIES

A. Magnetization curves

Referring to the magnetization curve of Fig. 1, several features are noteworthy. The initial portion of the magnetization curve is linear and reflects the perfect diamagnetic behavior of the sample at low field. Beyond H_{c1}, flux begins to penetrate the specimen thus polarizing the Er moments in the vortex cores. This polarization provides a positive contribution to the magnetization which eventually overcomes the negative contribution from the diamagnetic shielding currents and causes the magnetization to cross the $M=0$ axis. At the applied field where

$$(H_a - 4\pi n M) = H_{c2} ,$$

the magnetization suffers a change in slope, superconductivity is destroyed, and the specimen enters the paramagnetic phase.

Many of the features discussed above are more sharply evident in the associated susceptibility curve. For example, the initial Meissner region appears as a region of constant negative susceptibility. The field at which the susceptibility goes through zero corresponds to the maximum of the diamagnetic magnetization. At higher fields the sudden change in susceptibility signals the destruction of superconductivity, and marks the value of H_{c2}. At still higher fields, saturation effects are evident as the susceptibility becomes progressively smaller.

B. First-order phase transition at H_{c2}

The most interesting aspect of the magnetization curves in the magnetically easy $\bar{a}$ direction is the occurrence of a first-order phase transition into the normal state at H_{c2} in the temperature range $3.3\ \text{K} \geq T > T_f$. The magnetization curves show signs of the impending first-order transition even for $T > 3.3$ K by displaying an unusual downward curvature between H_{c1} and H_{c2}. Figure 3 shows the virgin magnetization curves for several temperatures. Even at $T=6.5$ K, the magnetization curve is not typical of type-II behavior since the slope increases as H_{c2} is approached. This is due to the increasing contribution of the Er moments to magnetization as their participating number grows in proportion to the normal fraction of the sample.

As the temperature is lowered, the moments become increasingly polarizable, hence the downward curvature becomes more pronounced and finally at $T \approx 3.3$ K the slope reaches the limiting value of $1/n=3$ which for a spherical sample is the analog of a discontinuity in M and the signature for a first-order phase transition. This behavior is more dramatically evident when the curves of Fig. 3 are redrawn in Fig. 4 to depict the magnetization M versus H_i which are the curves one obtains for a needle-shaped specimen for which $n=0$. Now, the first-order transition for $T=3$ K is seen as a discontinuity ΔM in magnetization at H_{c2}. Figure 5 shows several other virgin curves for temperatures between 3.0 and 0.5 K. These curves all display the limiting slope of $1/n=3$ at H_{c2}.

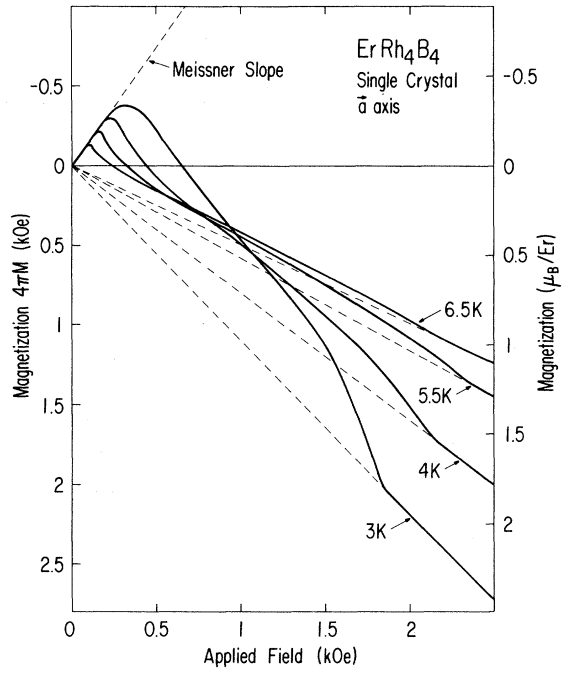

FIG. 3. Virgin magnetization curves for several temperatures. The external field is along the $\bar{a}$ direction.

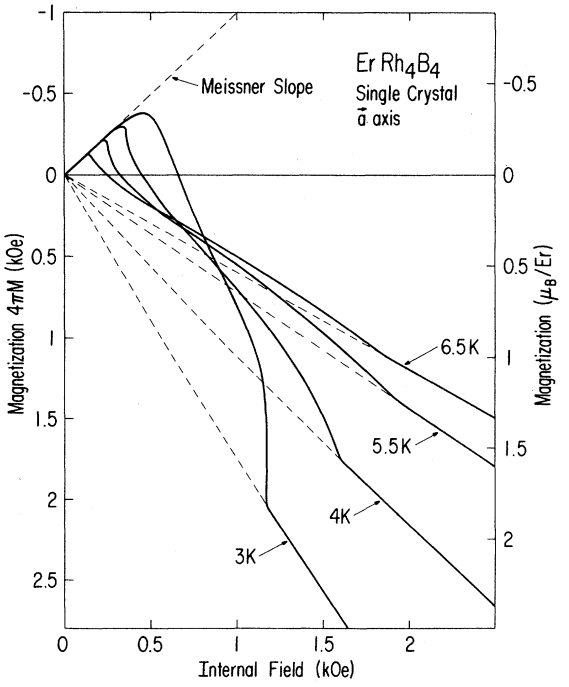

FIG. 4. Curves of Fig. 3 redrawn to give the magnetization vs the internal field. These are the magnetization curves one obtains for a needle-shaped specimen for which the demagnetization factor is 0.

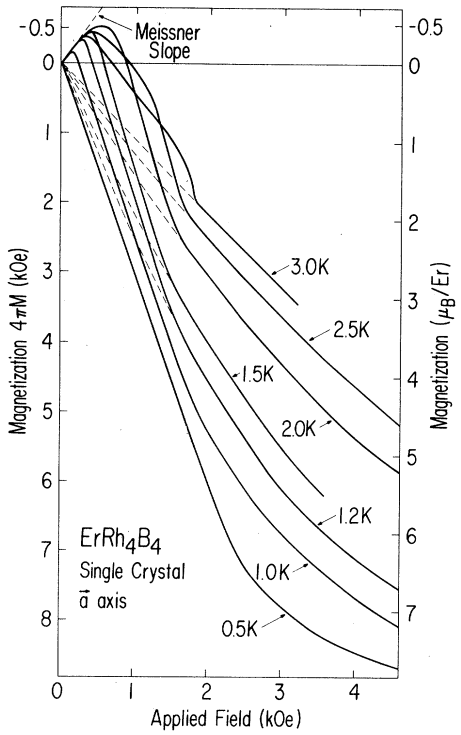

FIG. 5. Several more virgin magnetization curves for $T=3$ K and lower. These curves all display the limiting slope of $1/n=3$ at H_{c2} which is the signature for a first-order transition.

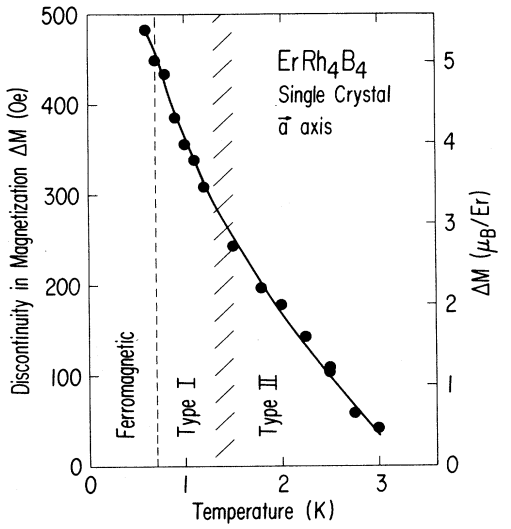

FIG. 6. Discontinuity in magnetization vs temperature.

The temperature dependence of the discontinuity in the magnetization is shown in Fig. 6. This discontinuity begins at 3.3 K, grows steadily and occurs at lower fields as the temperature is lowered. At about 1.4 K, the discontinuity begins to occur in the Meissner region, causing the crystal to behave like a type-I superconductor. With further decreases in temperature, the discontinuity grows further and moves through the Meissner region to lower fields. Finally at T_f the critical field falls to zero, superconductivity disappears, and the discontinuity becomes the spontaneous moment in the ferromagnetic state. As is evident in Fig. 6 the magnitude of the discontinuity in magnetization varies perfectly smoothly throughout these changes of phase, indicating a continuous and orderly evolution of the system from one state to the next as the temperature is lowered. Thus the appearance of a first-order phase transition at H_{c2} is the initial step of the reentrance process eventually leading to coexistence and ferromagnetism.

It is worthy to note that the evolution of $ErRh_4B_4$ from a type-II to a type-I superconductor does not follow the pattern of nonmagnetic superconductors, nor that expected of magnetic superconductors on the basis of the electromagnetic interaction between the localized Er moments and the superconducting electrons. In both of these cases a first-order transition, should it occur, initially appears at H_{c1} while the transition at H_{c2} remains second order. This is because when the Ginzburg-Landau equations are modified to include a paramagnetic normal state, a simple scaling rule emerges where the modified Ginzburg-Landau parameter κ' is related to the standard nonmagnetic κ through

$$\kappa'=\frac{\lambda'}{\xi}=\frac{\lambda}{\xi(1+4\pi\chi)^{1/2}}=\frac{\kappa}{(1+4\pi\chi)^{1/2}} .$$

Here λ is the penetration depth, ξ is the coherence distance, and χ is the magnetic susceptibility. Since χ grows as the temperature is lowered, κ' decreases with temperature allowing the system to transform into a type-I superconductor. However, we note that χ decreases with increasing field due to saturation effects. Hence, at constant temperature, κ' grows with increasing field producing a stronger tendency to type-II behavior as H_{c2} is approached. That is, a first-order phase transition at H_{c2} is not favored if only the electromagnetic interaction is considered. In $ErRh_4B_4$, however, the first-order transition initially appears at H_{c2} and moves to lower fields as the temperature falls, eventually merging with the transition at H_{c1} and producing type-I behavior. Thus the experimental results suggest that other mechanisms such as an exchange interaction between the local moments mediated through the conduction electrons—the so-called s-f exchange interaction—must be invoked to explain the behavior of the $ErRh_4B_4$ system.[8]

The magnitude of the discontinuity is related to the latent heat through the relation

$$L(T)=T\Delta M\,(dH_{c2}/dT) .$$

Since for the entire temperature range for which ΔM is nonzero, dH_{c2}/dT is positive (see Fig. 9) heat is given off when the crystal makes the first-order transition into the normal state. In other words, the normal state is the one with lower entropy compared with the superconducting state in presence of a field. This is contrary to what happens in type-I superconductors where at H_c an isothermal first-order transition into the normal state is as-

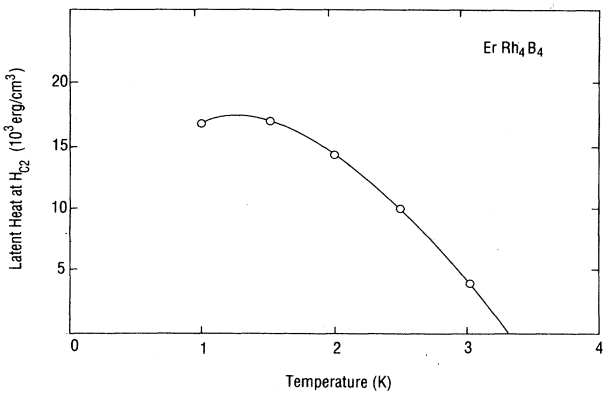

FIG. 7. Latent heat vs temperature for the transition from the superconducting to the normal state at H_{c2}.

sociated with absorption of heat. Figure 7 gives the value of latent heat L as a function of temperature for the transition into the normal state at H_{c2}. Note that this behavior persists even below 1.4 K when the specimen behaves like a type-I superconductor. Evidently the entropy of the normal state is lowered due to the ordering of Er moments in presence of the external field.

C. Magnetic anisotropy

The great magnetic anisotropy of the system becomes evident when the magnetization curves for the $\bar{c}$ and $\bar{a}$ directions are compared. Figure 8 shows the magnetization curves for the $\bar{c}$ axis at several temperatures. It is evident that apart from the weak paramagnetism which manifests itself at high fields, the $\bar{c}$-direction magnetization data display ordinary type-II superconducting behavior down to about 1.5 K. However, near the magnetic phase transition, even the $\bar{c}$-direction magnetization curves exhibit some novel features which are due to the increasing prominence of the magnetic effects in the coexistence region and will be discussed shortly.

The superconducting critical fields H_{c1} and H_{c2} are shown in Fig. 9 as functions of temperature for the $\bar{a}$ direction. The $\bar{c}$-direction data are shown in Fig. 10. The H_{c1} curve for the $\bar{c}$ direction is similar to that for the $\bar{a}$ direction and is deleted in the interest of clarity. The most noteworthy feature of the upper critical field curves is the presence of the nearly fivefold anisotropy in magnitude of H_{c2} between $\bar{a}$ and $\bar{c}$ directions. Furthermore for $T > 1.1$ K, the curve associated with the $\bar{c}$ direction is very nearly parabolic, a characteristic which is typical of ordinary type-II superconductors. On the other hand, H_{c2} versus T for the $\bar{a}$ direction reaches a maximum at 4.5 K, and begins a gradual decline to reach zero at T_f. In contrast the decline of H_{c2} in the $\bar{c}$ direction is sharp and occurs around $T \approx 1.1$ K, where the crystal enters a coexistence phase.

As noted earlier, the phase transition at H_{c2} in the $\bar{a}$ direction changes from second to first order when $T \leq 3.3$ K. Hence the H_{c2}-T phase boundary for the $\bar{a}$ direction contains a tricritical point at $T = 3.3$ K. On theoretical grounds, the existence of yet another tricritical point along the H_{c1}-T phase boundary has been suggested, but its experimental verification is difficult due to flux pinning problems at H_{c1}. A fuller discussion of these points and other novel features of the phase diagram appears elsewhere.[9]

In Fig. 11, we plot the critical magnetic induction B_{c2} defined as

$$B_{c2} = H_{c2} + 4\pi M_{c2}$$

versus temperature for both $\bar{a}$ and $\bar{c}$ directions. The B_{c2} curve associated with the $\bar{c}$ direction is very similar to the one for H_{c2} since the susceptibility is small and constant.

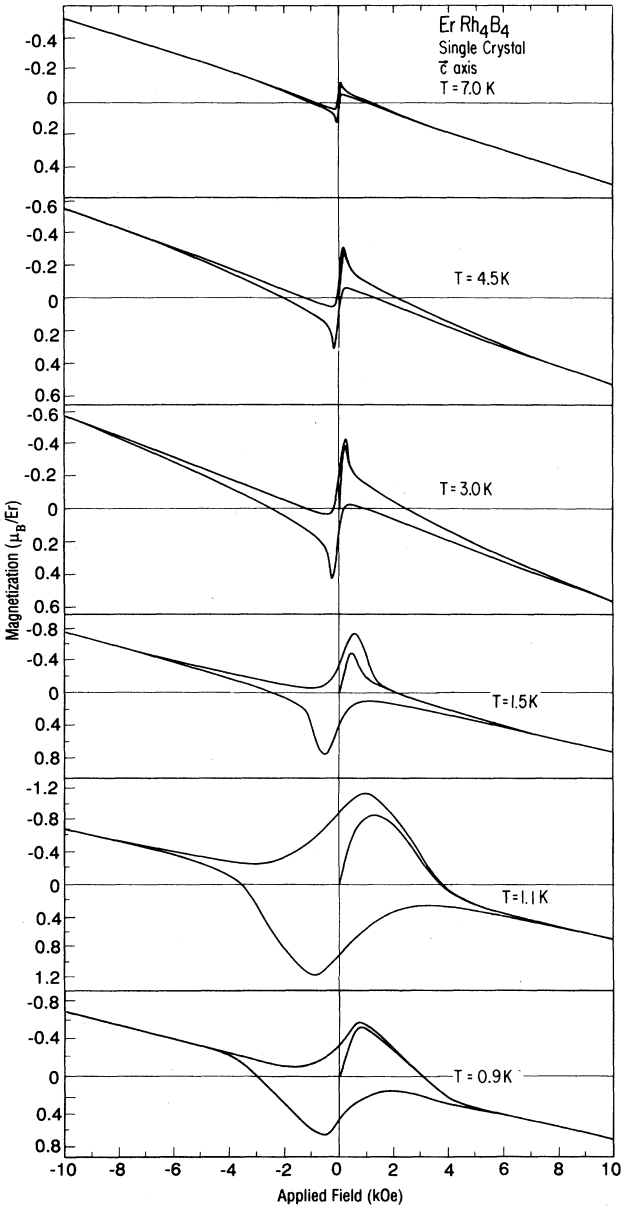

FIG. 8. Magnetization curves for several temperatures. The external field is parallel to the $\bar{c}$ axis of the crystal.

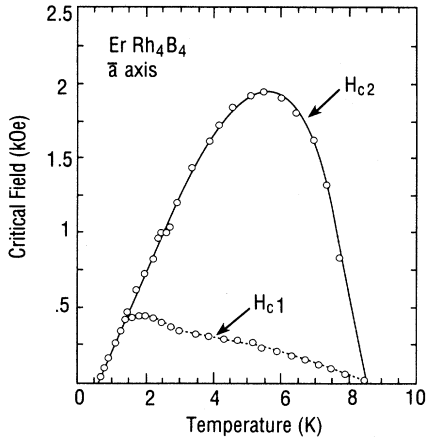

FIG. 9. Critical fields H_{c1} and H_{c2} vs temperature for the $\bar{a}$ direction.

However, the $\bar{a}$-direction curve for B_{c2} is highly unusual and shows complex behavior. The extent to which the B_{c2} curves differ in the two directions manifests the large role played by the magnetic moments in determining the $\bar{a}$-direction superconducting behavior of the system. Indeed in the $\bar{a}$ direction, the contribution to the local field comes from the usual $(H_{c2}+4\pi M)$ term plus the added contribution due to the exchange field. If the local field needed to destroy superconductivity is assumed to be the same for both directions, then the difference in B_{c2} between the two directions is, in the mean-field theory sense, a measure of the contribution of the exchange interaction to the local field.

D. Coexistence of superconductivity and ferromagnetism

Neutron scattering experiments on a single-crystal specimen have revealed a region of coexistence in the temperature range $1.1 > T > 0.7$ K. In this range, it is thought that in addition to normal ferromagnetic regions which may arise due to strain, superconducting and

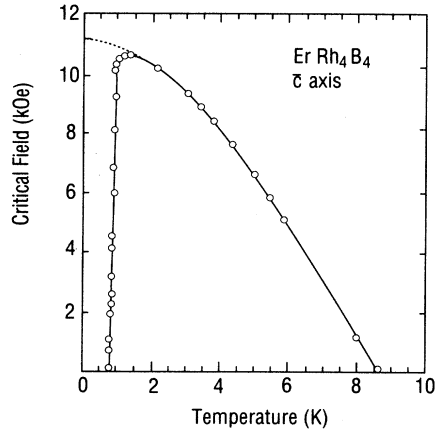

FIG. 10. Upper critical field H_{c2} vs temperature for the $\bar{c}$ direction.

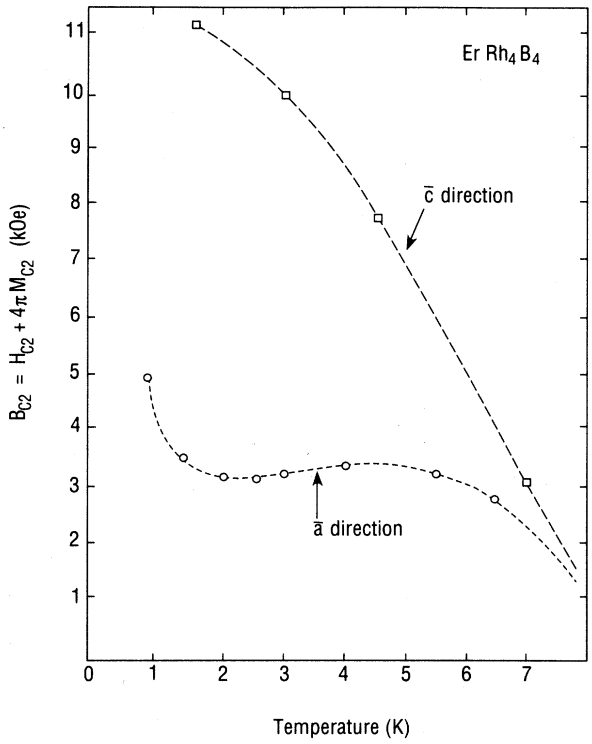

FIG. 11. Critical magnetic induction B_{c2} vs temperature for both $\bar{a}$ and $\bar{c}$ directions.

sinusoidally modulated ferromagnetic states coexist in certain other nonstrained regions. Our data indicate that this temperature range is also associated with an incomplete Meissner state, characterized by a gradual decrease in the Meissner slope as the temperature is lowered from 1.1 toward 0.7 K. Figure 12 shows the Meissner slope versus temperature for $T > T_f$. The plot displays a rather sharp decline at $T \approx 1.1$ K where the lower slope may be interpreted to result from a gross division of the crystal into normal and coexistence regions. Since the coexistence regions exhibit the complete Meissner effect, the bulk ratio of the normal to the coexistence regions can be estimated by using the data in the $\bar{c}$ direction where fortuitously the normal state susceptibility χ_n is found to be constant below $T = 15$ K.

The total susceptibility χ is the sum of the contributions from normal and superconducting regions in proportion to their bulk ratio. That is,

$$\chi = -[(1-\eta)/4\pi] + \eta\chi_n \ ,$$

where η is the normal fraction, hence

$$\eta = (1+4\pi\chi)/(1+4\pi\chi_n) \ .$$

Since in this expression the denominator is a constant, the graph of η versus temperature is identical to a plot of χ versus T, except for a scale factor. This is shown as the right-hand scale in Fig. 12. Clearly, the normal fraction η begins to increase below 1.1 K. At 1 K the normal fraction is about 5%, growing rapidly to 20% by 0.8 K, to 50% by 0.75 K, and reaching 100% by $T_f = 0.7$ K.

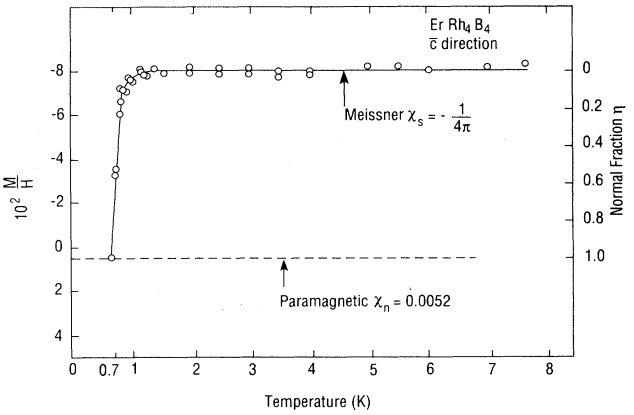

FIG. 12. Meissner slope vs temperature for $T > T_f$. The ordinate M/H is in dimensionless units.

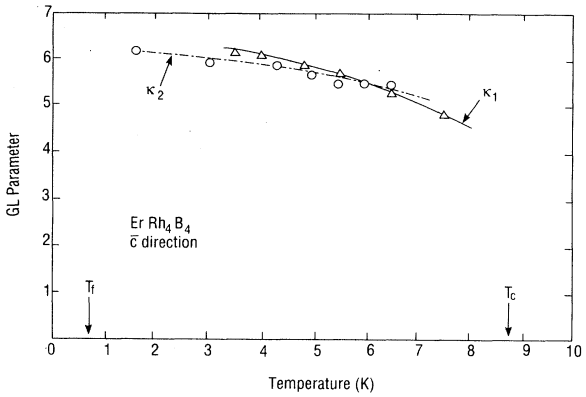

FIG. 13. Ginzburg-Landau parameters κ_1 and κ_2 as functions of temperature for the $\bar{c}$ direction.

E. Ginzburg-Landau parameters

As mentioned earlier, the superconducting magnetization curves in the $\bar{c}$ direction, apart from a small and constant normal susceptibility, display features similar to type-II superconductors. It is therefore of some interest to obtain the temperature dependence of the superconducting Ginzburg-Landau parameters κ_1 and κ_2 from the $\bar{c}$-direction data. In obtaining κ_1 and κ_2 from the magnetization curves, the small but finite normal state susceptibility must be taken into account. We follow the self-consistent formulation of κ_1 and κ_2 suggested by Matsumoto *et al.*,[10] which is valid for magnetic superconductors independent of specific model or the form of interaction. In analogy with the nonmagnetic case, κ_1 is defined as

$$\kappa_1 \equiv B_{c2}/(\sqrt{2}H_c) ,$$

where H_c is the thermodynamic critical field, and

$$B_{c2} = H_{c2} + 4\pi M_{c2} .$$

Similarly in analogy with the nonmagnetic case, κ_2 is defined through the relation

$$4\pi(\chi_s - \chi_n)_{H_{c2}} = (1+4\pi\chi_n)_{H_{c2}}/\{\beta[2\kappa_2^2/(1+4\pi\chi_n)-1]\} ,$$

where $\chi_s \equiv dM_s/dH_i$ and $\chi_n \equiv dM_n/dH_i$ are the superconducting and normal susceptibilities and $\beta = 1.16$ for a triangular vortex lattice.

In Fig. 13, plots of κ_1 and κ_2 are shown as functions of temperature for the $\bar{c}$ direction. It is observed that near T_c, $\kappa_1 \cong \kappa_2 \cong 4.5$. The variation of κ_1 and κ_2 with temperature are similar to ordinary type-II superconductors, *increasing* by $\approx 20\%$ at low temperatures compared to the value at T_c. When the interaction between the local Er moments (due to the $4f$ electrons) and the conduction electrons is primarily electromagnetic (i.e., in the absence of the so-called s-f exchange interaction) one can estimate the value of bare κ in the absence of magnetic interaction by a simple scaling where $\kappa_{\text{bare}} = \kappa(B_{c2}/H_{c2})^{1/2}$. This correction results in about 3% increase in the $\bar{c}$-direction values of κ_1 and κ_2.

In the $\bar{a}$ direction, only the values of $\kappa_1 = B_{c2}/(\sqrt{2}H_c)$ can be estimated reliably. This is due to the fact that to evaluate κ_2, one needs to determine the slope of the magnetization curves near H_{c2}. As was noted earlier, the magnetization curves in the $\bar{a}$ direction exhibit a downward curvature between H_{c1} and H_{c2} which becomes increasingly severe as the temperature is lowered. This trend leads to the onset of a first-order phase transition at H_{c2} below 3.3 K and translates into a *decreasing* value of κ_2 as the temperature is lowered.

Figure 14 shows κ_1 and κ_2 versus temperature for the $\bar{a}$ direction. Note that unlike type-II superconductors, κ_1 *decreases* as the temperature is lowered and extrapolates to a value of $(1/\sqrt{2})$ at 1.4 K when the system transforms to a type-I superconductor. If the scaling correction $\kappa_{\text{bare}} = \kappa(B_{c2}/H_{c2})^{1/2}$ is applied to estimate the value of bare κ, one obtains a value of $\kappa \approx 4.5$ at T_c, consistent with that in the $\bar{c}$ direction, but the temperature dependence of κ_{bare} remains anomalous, i.e., κ_{bare} decreases as the temperature is lowered. This behavior indicates that the s-f exchange interaction plays an important role in determining the magnetic behavior of the system along the $\bar{a}$ axis. Figure 14 also shows κ_2 versus temperature obtained from the $\bar{a}$-direction magnetization curves. Despite the anomalous nature of the magnetization curves, the values of κ_2 are generally consistent with those for κ_1 and follow the same decreasing trend as the temperature is lowered. Indeed, κ_2 approaches a constant value of $1/\sqrt{2}$ which is characteristic of type-I superconductors as the temperature nears 1.4 K and remains at this value for $T_f < T < 1.4$ K. The fact that κ_2 approaches the value of $1/\sqrt{2}$ is merely a reflection of the onset of the type-I behavior at 1.4 K.

In ordinary type-II superconductors, a third parameter κ_3 is given by

$$\kappa_3 = (\sqrt{8}H_c\pi\lambda^2)/\phi_0 , \quad (1)$$

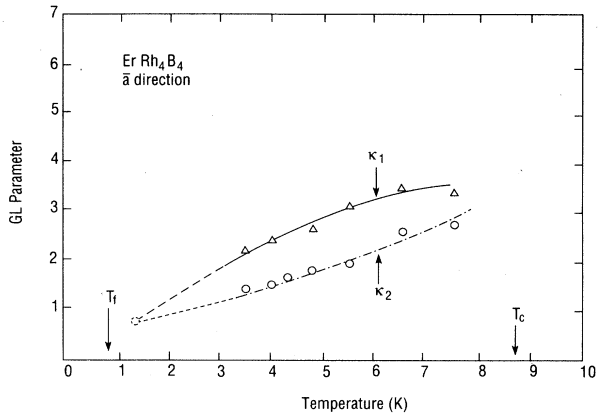

FIG. 14. Ginzburg-Landau parameters κ_1 and κ_2 vs temperature for $\bar{a}$ direction.

where ϕ_0 is the flux quantum, and λ is the penetration depth. Near the transition temperature T_c, we have

$$\lambda(t)=1/\sqrt{2}\lambda_L(1-t)^{-1/2} \tag{2}$$

and

$$\kappa=\kappa_1=\kappa_2=\kappa_3=\frac{\lambda}{\xi}\ , \tag{3}$$

where ξ is the Ginzburg-Landau coherence length and t is the reduced temperature. Here λ_L is the London penetration depth and κ is the G-L parameter. When Eqs. (2) and (3) are substituted in Eq. (1) and the result differentiated with respect to t, one obtains

$$\lambda_L=[\phi_0\kappa/(\pi\sqrt{2}|dH_c/dt|_{T_c})]^{1/2}\ . \tag{4}$$

Note that all the quantities on the right-hand side of Eq. (4) are determined experimentally. Once λ_L is determined, the value of the BCS coherence length ξ_0 can be estimated by noting that $\kappa\cong 0.96\lambda_L(0)/\xi_0$ in the pure limit.

Although the above relations are valid for ordinary type-II superconductors, one may apply them with caution to the $\bar{c}$-axis data (where the effect of local magnetism is very mild) to obtain an estimate of the superconducting parameters $\lambda_L(0)$ and ξ_0. Our data yield $\lambda_L(0)\cong 830$ Å and $\xi_0\cong 180$ Å for the $\bar{c}$ direction.

An estimate of $\xi(0)$, the Ginzburg-Landau coherence length at $T=0$, can be obtained by noting that for a triangular vortex array, $B_{c2}=\phi_0/2\pi\xi^2$. For the $\bar{c}$ direction the upper critical field H_{c2} and hence B_{c2} follow a nearly parabolic dependence on temperature down to about 1.5 K. Extrapolation of H_{c2} to $T=0$ gives a value for $H_{c2}(0)\approx 11$ kG, which in turn gives $B_{c2}(0)=11(1+4\pi\chi_n)\cong 11.7$ kG. This then leads to $\xi(0)\cong 170$ Å which is quite consistent with the value for $\xi_0=180$ Å obtained above because in pure superconductors $\xi(0)=0.74\xi_0$. Furthermore, since $\kappa=\lambda/\xi=4.5$, assuming $\xi(0)=170$ Å, we obtain an estimate for $\lambda(0)\cong 765$ Å.

The question of whether or not the parameters κ_1 and κ_2 are of any real significance in magnetic superconductors should be examined. In their original form these parameters were defined for ordinary type-II superconductors with no abnormal features in their magnetization curves. Broadly speaking, both parameters reflect the ratio of H_{c2}/H_c. This is because κ_1 is defined as $H_{c2}/(\sqrt{2}H_c)$, and the value of κ_2 is proportional to $[(dM/dH)_{H_{c2}})]^{-1/2}$. Note that for a given thermodynamic critical field H_c (i.e., fixed condensation energy), κ_1 increases proportionally with H_{c2}. Similarly, κ_2 gets large when the slope $(dM/dH)|_{H_{c2}}$ gets small due to larger H_{c2}.

These considerations do not apply to materials with anomalous magnetization curves. Our data indicate that the $\bar{c}$-direction magnetization curves are similar to the ordinary type-II case and therefore one may ascribe some relevance to the values of κ_1 and κ_2 obtained from the $\bar{c}$-direction data. The magnetization curves for the $\bar{a}$ direction, however, are quite anomalous and cannot be used to obtain κ_1 and κ_2 reliably. Since $\kappa_1=H_{c2}/(\sqrt{2}H_c)$, and the H_{c2} versus temperature curve for the $\bar{a}$ direction is severely affected by the large susceptibility one can expect κ_1 to reflect this anomalous behavior as well. Furthermore, the evaluation of κ_2 for the $\bar{a}$ direction is unsatisfactory as the slope of the magnetization curves near H_{c2} are quite anomalous. Nevertheless, it is a surprising fact that if one adheres strictly to the procedure for determining κ_1 and κ_2 for the $\bar{a}$-direction data, the results are at least consistent. As Fig. 14 shows, both κ_1 and κ_2 show a *decrease* as the temperature is lowered approaching a value close to $1/\sqrt{2}$ at about 1.4 K where the specimen exhibits type-I behavior.

IV. NORMAL-STATE MAGNETIC BEHAVIOR

In this section we briefly review the magnetic behavior of the system in the paramagnetic and ferromagnetic phases. As mentioned earlier, $ErRh_4B_4$ is a paramagnet for $T>T_c=8.6$ K. We have previously reported in detail on the system's paramagnetic properties and explained the data in terms of a combined crystalline electric field and molecular field approach.[4] Here we describe the normal magnetic behavior of the sample for $T<T_c$.

The magnetic response of the system is masked by the superconducting phase for $T_c>T>T_f$. However, for fields greater than the superconducting critical field, the magnetic response is directly observable without the intrusion of superconductivity. Further, the high-field magnetization data can be extrapolated to infer the bare magnetic response of the system below the critical field where ordinarily superconductivity masks the effect.

To this end, one notes that neglecting volume changes, the normal state Helmholtz free energy is given by

$$F(T,M)=F_0(T)+\frac{\alpha(T)}{2}M^2+\frac{\beta(T)}{4}M^4+\frac{\gamma(T)}{6}M^6+\cdots\ ,$$

where α, β, and γ are known as the magnetic Landau parameters. Since

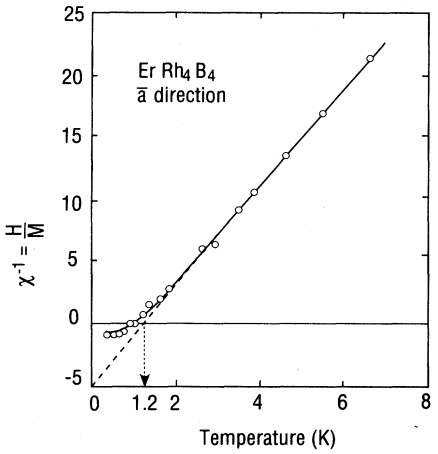

FIG. 15. Curie-Weiss plot from $\bar{a}$-direction magnetization data. The ordinate H/M is in dimensionless units.

$$H=\frac{\partial F}{\partial M}=\alpha(T)M+\beta(T)M^3+\gamma(T)M^5+\cdots ,$$

we may fit the experimental magnetization curves above H_{c2} to this expression to obtain the normal magnetization below H_{c2}.

Figure 15 is a Curie-Weiss plot which shows $\alpha(T)$ versus temperature. The dashed line is a straight line fit of the form $\alpha=A(T-T_m)$, with $A=5.83\ \mathrm{K}^{-1}$ and $T_m=1.2$ K. T_m should be viewed as the *bare* Curie point which would signal the ferromagnetic ordering temperature in the absence of superconductivity. A more extensive account of the Landau parameters will be published elsewhere.

For $T_f<T<T_m$, one observes a coexistence region where superconductivity and long-range magnetic order appear to coexist as discussed earlier. At $T_f=0.7$ K, the last traces of superconductivity disappear and the magnetization curves in $\bar{a}$ direction show a large spontaneous moment characteristic of ferromagnetic order.

Figure 16 shows the induced moment per Er atom as a function of the internal field H_i for both directions at temperatures well below T_f. The great anisotropy in the magnetic response between the two directions is clearly evident here. The $\bar{c}$-direction data indicate a weak paramagnet with a small induced moment which increases linearly with field. In marked contrast, the $\bar{a}$-direction data show a large spontaneous moment characteristic of a ferromagnet at zero field, thus confirming that the Er moments are confined to the basal plane, and easily polarized along $\bar{a}$.

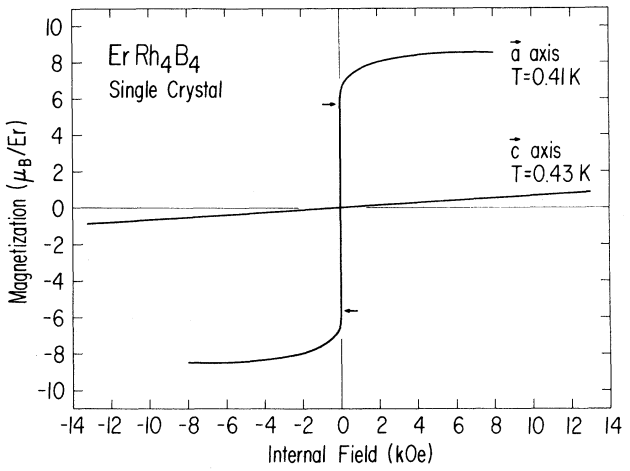

FIG. 16. Induced moment per Er atom as a function of the internal field for both $\bar{a}$ and $\bar{c}$ directions in the ferromagnetic phase. The arrows indicate the spontaneous moment at $T=0.41$ K.

Further, the $\bar{a}$-direction data in Fig. 16 show ideal ferromagnetic behavior with the magnetization rising smoothly from a spontaneous value of $5.7\pm2\ \mu_B$/Er at zero internal field to a saturation value of $8.5\pm0.1\ \mu_B$/Er at 7 kOe internal field. The arrows in Fig. 16 indicate the value of the spontaneous moment where the magnetization curve begins to deviate from the vertical $H_i=0$ axis. Although this feature is difficult to see in Fig. 16, it is clearly evident in the raw data where the magnetization is recorded as a function of the applied field H_a.

The complete absence of hysteresis in the $\bar{a}$-direction data indicates that the magnetic domain boundaries move freely as the applied field is varied. The free movement of the domain boundaries is consistent with the mild hysteresis in the superconducting phase, and implies a low concentration of defects in the specimen which may serve as pinning centers.

The $\bar{a}$-direction spontaneous and saturation moments are in excellent agreement with values measured by neutron scattering[2] (5.6 μ_B/Er) and Mossbauer effect[11] (8.3 μ_B/Er). Our measurements thus reconcile this basic discrepancy, and suggest that a neutron measurement of the saturation moment would agree with the Mossbauer result.

ACKNOWLEDGMENTS

This work was supported by the U.S. Department of Energy, Basic Energy Sciences–Material Sciences, under Contract No. W-31-109-ENG-38.

*Permanent address: Department of Physics, University of Wisconsin, Kenosha, WI 53141.
†Current address: Boeing Aerospace Co., Seattle, WA 98124.

[1]D. C. Johnston and H. F. Baun, in *Superconductivity in Ternary Compounds II,* edited by M. B. Maple and O. Fischer (Springer-Verlag, Berlin, 1982), pp. 10–55.
[2]S. K. Sinha, G. W. Crabtree, D. G. Hinks, and H. Mook, Phys. Rev. Lett. **48**, 950 (1982).
[3]J. W. Lynn, G. Shirane, W. Thomlinson, and R. N. Shelton, Phys. Rev. Lett. **46**, 368 (1981).
[4]B. D. Dunlap, L. N. Hall, F. Behroozi, G. W. Crabtree, and D. G. Niarchos, Phys. Rev. B **29**, 6244 (1984).
[5]G. W. Crabtree, F. Behroozi, S. A. Campbell, and D. G. Hinks, Phys. Rev. Lett. **49**, 1342 (1982).

[6]*Superconductivity in Ternary Compounds,* edited by O. Fischer and M. B. Maple (North-Holland, Amsterdam, 1982).
[7]F. Behroozi, Am. J. Phys. **51**, 28 (1983).
[8]T. Koyama, M. Suzuki, O. Sakai, S. Maekawa, and M. Tachiki, J. Magn. Magn. Mater. **31-34**, 505 (1983).
[9]G. W. Crabtree, R. K. Kalia, D. G. Hinks, F. Behroozi, and M. Tachiki, J. Magn. Magn. Mater. **54-57**, 703 (1986).
[10]M. Matsumoto, H. Umezawa, and M. Tachiki, Phys. Rev. B **25**, 6633 (1982).
[11]G. K. Shenoy, B. D. Dunlap, F. Y. Fradin, S. K. Sinha, C. W. Kimball, W. Potzel, F. Probst, and G. M. Kalvius, Phys. Rev. B **21**, 3886 (1980).